

Interleaved Soft-Switching Buck Converter with Coupled Inductors

Cheng-Tao Tsai

Department of Electrical Engineering
National Chin-Yi University of Technology
No. 35, Lane 215, Sec. 1, Chung-Shan Rd,
Taiping City, Taichung,
Taiwan, 411

E-mail: ctsai@ncut.edu.tw

<http://web2.ncut.edu.tw/bin/home.php>

Chih-Lung Shen

Department of Electronic Engineering
National Kaohsiung First University of Science
and Technology
No. 1 University Road, Yuanchau, Kaohsiung,
Taiwan, 811

E-mail: clshen@ccms.nkfust.edu.tw

<http://www.nkfust.edu.tw/>

Abstract: - This paper presents an interleaved soft-switching buck converter with coupled inductors to extend duty ratio for high step-down voltage applications. In the proposed converter, a single-capacitor turn-off snubber is introduced to limit voltage rising rate of active switches to reduce turn-off loss. To handle the energy trapped in the leakage inductance of the coupled inductors, simple passive-clamp circuits are added to the proposed converter, which can effectively recycle the energy and suppress voltage spike. To highlight the merits of the proposed converter, its performance indexes, such as voltage gain function and component stresses, are analyzed and compared with those of the conventional interleaved buck converter. In this study, a prototype of the proposed converter, of which input voltage range is 127-177 V_{dc}, output voltage is 12 V_{dc}, and power capacity rates at 240 W, has been designed and implemented to verify the feasibility. From experimental results, it has been shown that conversion efficiency up to 85% can be achieved at full load condition.

Key-Words: - Interleaved, soft-switching, coupled inductors, leakage inductance, passive-clamp circuits.

1 Introduction

Interleaved buck converter (IBC) is widely adopted in step-down voltage, high power density, low output current ripple, and non-isolated applications [1]-[9]. However, as the switching frequencies being increased, switching loss, noise and stress associated with turn-on and turn-off transitions are also increased. These drawbacks reduce power conversion efficiency and powering capability, which in turn seriously deteriorate in system performance. To overcome the above-discussed drawbacks, IBC with a single-capacitor turn-off snubber was proposed to achieve soft-switching function [10], as shown in Fig. 1. Although it can reduce turn-off loss of active switch and component count of passive snubber, its efficiency is not attracted at high step-down voltage applications. The reason is that it suffers from extremely low duty ratio and high component stress. For example, when input voltage is 156 V_{dc} (110V_{ac}) and output voltage is 12 V_{dc}, its duty ratio is only 0.077 and conversion efficiency is only about 74%. Additionally, reverse-recovery problems of the free-wheeling diodes become severe issues when the input voltage goes beyond a high level and there are no proper Schottky diodes available. The reverse-recovery current of the free-wheeling diodes has detrimental effects on the performance of the IBC. When the

IBC with a single-capacitor turn-off snubber is operated in continuous-conduction mode (CCM), high switching loss resulting from the reverse-recovery current dramatically deteriorates the thermal condition of the free-wheeling diodes [11]-[16]. These drawbacks limit the IBC with a single-capacitor turn-off snubber from high step-down voltage and high power density applications.

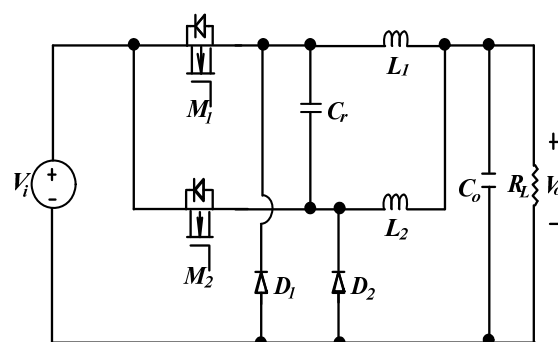


Fig. 1. Topology of IBC with a single-capacitor turn-off snubber.

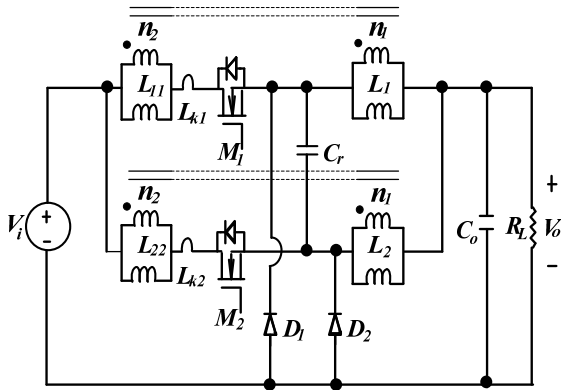


Fig. 2. Topology of the first version of the proposed converter.

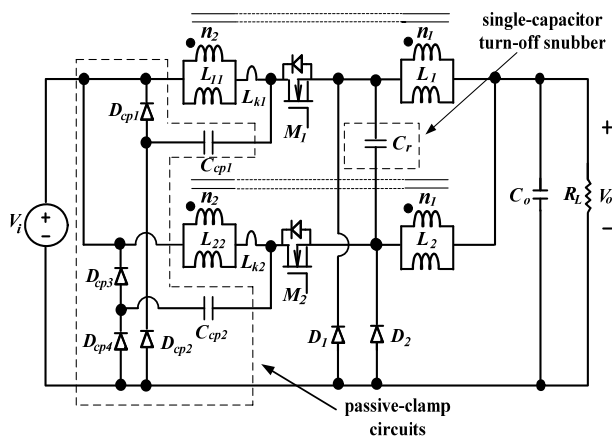


Fig. 3. Topology of the final version of the proposed converter embedding passive-clamp circuits.

To relieve the drawbacks, utilizing coupled inductors is a solution [11]-[13]. An IBC with coupled-inductor has simpler winding structure, and always transfers power to the output through the primary winding, reducing peak primary winding current. Thus, a converter with a coupled inductor is relatively attractive because the converter presents an extendable duty ratio and low diode voltage stress, which in turn can reduce reverse-recovery loss. In this paper, we first propose a coupled-inductor IBC with single capacitor snubber to yield high step-down voltage gain and reduce switching loss, as shown in Fig. 2. Nevertheless, the leakage inductance of the coupled inductors will resonate with the parasitic capacitance of the active switches, which not only increases the voltage stress of the active switches, but induces significant switching loss [13]-[15]. To handle the energy trapped in the leakage inductance, a simple passive-clamp circuit is introduced into the coupled-inductor IBC to derive the final version, as shown in Fig. 3. With the proposed interleaved coupled-buck converter (ICBC), which can effectively recycle the leakage energy, achieve

soft-switching feature and suppress voltage spike so that conversion efficiency can be improved significantly.

In this paper, operational principle and feature analysis of the soft-switching ICBC are described in Section 2. Section 3 presents design consideration and efficiency estimation of the ICBC, and its experimental results obtained from a prototype built with the proposed converter are presented in Section 4 to verify its feasibility. Finally, a conclusion is given in Section 5.

2 Operational Principle and Feature Analysis

As shown in Fig. 3, the proposed ICBC consists of two sets of coupled-buck converters, two sets of passive-clamp circuits and a single-capacitor turn-off snubber. The driving signals, current and voltage waveforms of its key components are shown in Fig. 4. In Fig. 3, each coupled inductor can be replaced with an equivalent transformer and two magnetizing inductors in this section.

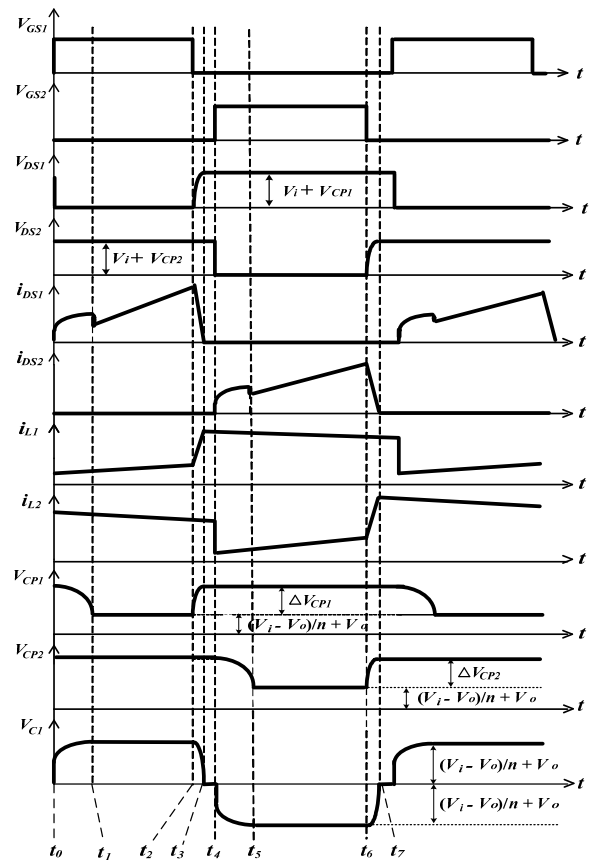


Fig. 4. Key waveforms of the proposed soft-switching converter.

2.1 Operational Principle

To simplify the description of the operational modes, the following assumptions are made.

- 1) Capacitances of C_o , C_{CP1} and C_{CP2} are large enough so that the voltages across them are constant over a switching period.
- 2) All of the switching devices, MOSFETs and diodes, are ideal.

Based on the above assumptions, operation of the proposed converter over one switching cycle can be divided into seven modes. Fig. 5 shows equivalent circuit modes of the proposed soft-switching converter over a switching cycle. Operation of the converter is explained mode by mode as follows:

Mode 1 [Fig. 5(a), $t_0 \leq t < t_1$]:

This mode begins when M_1 starts conducting at t_0 . Coupled inductors L_{11} and L_1 are linearly charged, and inductor current i_{L1} flowing through the path of $V_o-V_i-L_{11}-L_{k1}-M_1-L_1$ linearly increases. At the same time, clamp capacitor C_{CP1} is discharged and snubber capacitor C_r begins resonating with leakage inductance L_{k1} . During this interval, switch M_2 , clamp diodes D_{CP1} , D_{CP3} and D_{CP4} , and free-wheeling diode D_1 are in the off states. The energy stored in inductor L_{22} will be released to the load through coupled inductor L_2 , and inductor current i_{L2} flowing through the path of V_o-D_2 is decreased. The coupled inductor currents i_{L1} and i_{L2} can be expressed as follows:

$$i_{L1}(t) = \frac{V_i - V_o}{n^2 L_1} \times (t - t_0) + i_{L1}(t_0), \quad (1)$$

and

$$i_{L2}(t) = \frac{V_o}{n L_2} \times (t - t_0) + i_{L2}(t_0), \quad (2)$$

where V_i and V_o are input voltage and output voltage, and n is the turns ratio of the coupled inductors L_1 and L_{11} or L_2 and L_{22} .

Mode 2 [Fig. 5(b), $t_1 \leq t < t_2$]:

At time t_1 , the clamp capacitor C_{CP1} is discharged to a steady-state voltage value, V_{CP1} , and snubber capacitor C_r is completely charged. The clamp capacitor and snubber capacitor voltages can be derived as

$$V_{CP1} = V_{Cr} = \frac{(V_i - V_o)}{n} + V_o. \quad (3)$$

Mode 3 [Fig. 5(c), $t_2 \leq t < t_3$]:

At time t_2 , switch M_1 is turned off, and switch M_2 , clamp capacitors D_{CP3} and D_{CP4} as well as free-wheeling diode D_1 still stay in the off states. Snubber capacitor C_r begins discharging, and the energy trapped in leakage inductance L_{k1} is transferred to clamp capacitor C_{CP1} . If C_{CP1} is large enough and the increased voltage across C_{CP1} is relatively small, the voltage variation on clamp capacitor will be about

$$\Delta V_{CP1} = \frac{L_{k1} \times i_{DS1}^2}{2C_{CP1} \times V_{CP1}}. \quad (4)$$

Thus, the total voltage of C_{CP1} can be derived as

$$V_{CP1(total)} = \frac{(V_i - V_o)}{n} + V_o + \Delta V_{CP1}. \quad (5)$$

Mode 4 [Fig. 5(d), $t_3 \leq t < t_4$]:

In this mode, as the voltage of snubber capacitor C_r drops to zero, free-wheeling diode D_1 is conducted. The energy stored in inductor L_{11} will be released to the load through coupled inductor L_1 , and inductor current i_{L1} flowing through the path of V_o-D_1 is decreased. Coupled inductor currents i_{L1} and i_{L2} can be expressed as follows:

$$i_{L1}(t) = \frac{V_o}{n L_1} \times (t - t_3) + i_{L1}(t_3), \quad (6)$$

and

$$i_{L2}(t) = \frac{V_o}{n L_2} \times (t - t_3) + i_{L2}(t_3). \quad (7)$$

Mode 5 [Fig. 5(e), $t_4 \leq t < t_5$]:

At time t_4 , switch M_2 is conducting, coupled inductors L_{22} and L_2 are linearly charged, and inductor current i_{L2} flowing through the path of $V_o-V_i-L_{22}-L_{k2}-M_2-L_2$ linearly increases. Meanwhile, clamp capacitor C_{CP2} is discharged and snubber capacitor C_r begins resonating with leakage inductance L_{k2} . During this interval, switch M_1 , clamp diodes D_{CP1} , D_{CP2} and D_{CP3} , and free-wheeling diode D_2 are in the off states. The energy stored in inductor L_{22} will continue releasing to the load through coupled inductor L_2 . Coupled inductor currents i_{L1} and i_{L2} can be expressed as follows:

$$i_{L1}(t) = \frac{V_o}{n L_1} \times (t - t_4) + i_{L1}(t_4), \quad (8)$$

and

$$i_{L2}(t) = \frac{V_i - V_o}{n^2 L_2} \times (t - t_4) + i_{L2}(t_4). \quad (9)$$

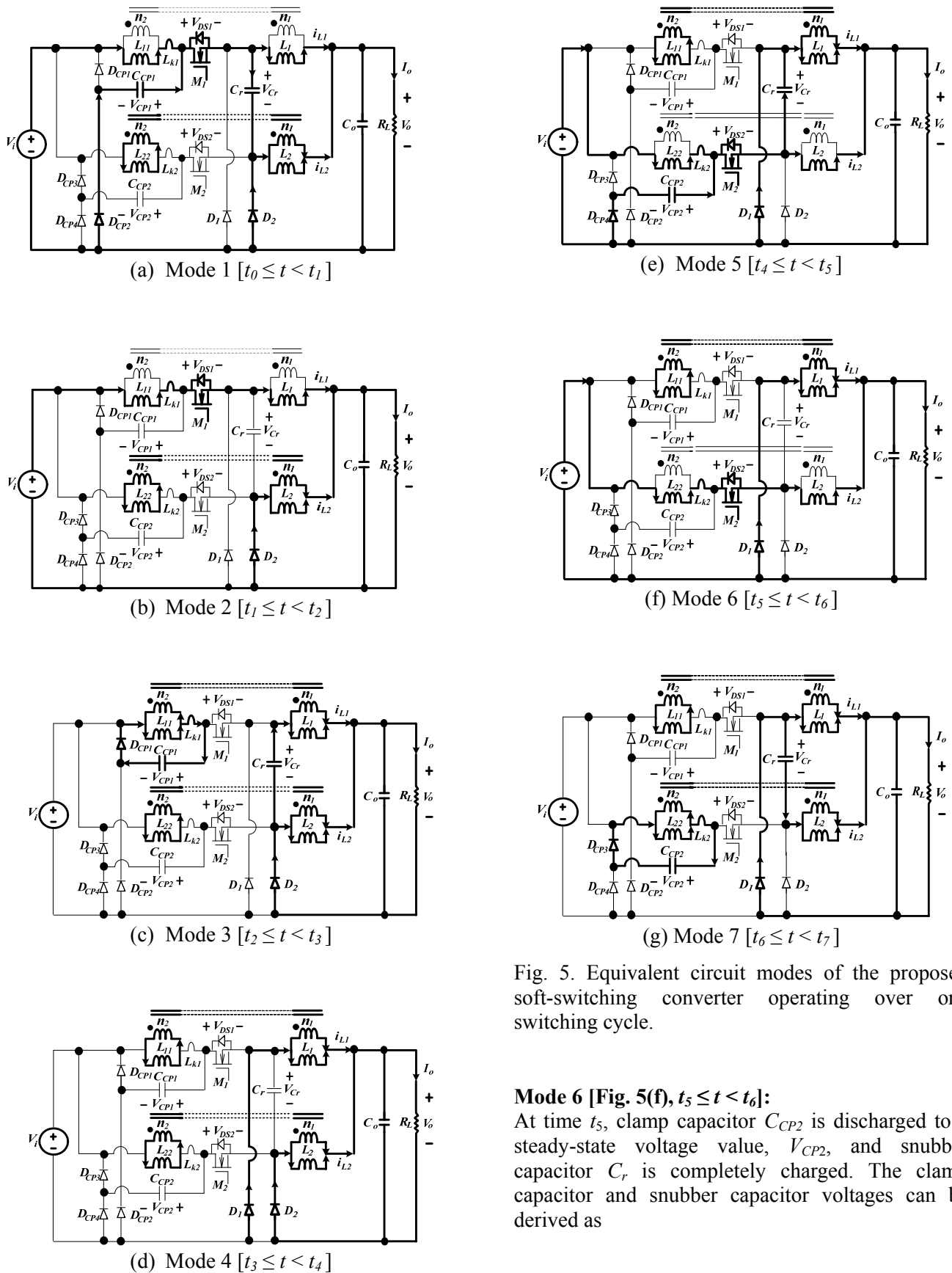


Fig. 5. Equivalent circuit modes of the proposed soft-switching converter operating over one switching cycle.

Mode 6 [Fig. 5(f), $t_5 \leq t < t_6$]:

At time t_5 , clamp capacitor C_{CP2} is discharged to a steady-state voltage value, V_{CP2} , and snubber capacitor C_r is completely charged. The clamp capacitor and snubber capacitor voltages can be derived as

$$V_{CP2} = V_{C2} = \frac{(V_i - V_o)}{n} + V_o. \tag{10}$$

Mode 7 [Fig. 5(g), $t_6 \leq t < t_7$]:

At time t_6 , switch M_2 is turned off, and switch M_1 , clamp capacitors D_{CP1} , D_{CP2} and D_{CP4} as well as free-wheeling diode D_2 still stay in the off states. Snubber capacitor C_r begins discharging, and the energy trapped in leakage inductance L_{k2} is transferred to clamp capacitor C_{CP2} . Suppose that C_{CP2} is large enough, the voltage increment on C_{CP2} will be relatively small and can be determined as

$$\Delta V_{CP2} = \frac{L_{k2} \times i_{DS2}^2}{2C_{CP2} \times V_{CP2}}. \quad (11)$$

As a result, the total voltage of C_{CP2} can be expressed by the following equation

$$V_{CP2(total)} = \frac{(V_i - V_o)}{n} + V_o + \Delta V_{CP2}. \quad (12)$$

When switch M_1 starts conducting again at the end of Mode 7, the converter operation over one switching cycle is completed.

2.2 Feature Analysis

The proposed soft-switching ICBC can extend duty ratio of the active switches and reduce component stress. This section describes the feature analysis for the proposed ICBC. The feature analysis includes voltage gain, duty ratio, and voltage stresses of diode and active switch.

2.2.1 Voltage Gain and Duty Ratio

From the key waveforms of the converter shown in Fig. 4 and by applying the volt-second balance criterion, the voltage gain and duty ratio can be derived as

$$\frac{V_o}{V_i} = \frac{D}{D + n(1 - D)}, (n \neq 0), \quad (13)$$

and

$$D = \frac{nV_o}{V_i + nV_o - V_o}, (D < 0.5), \quad (14)$$

where D is the duty ratio of the active switch.

For example, input voltage $V_i = 127\text{-}177 \text{ V}_{dc}$ (90-125 V_{ac}) and output voltage $V_o = 12 \text{ V}_{dc}$ are considered. From (13) and (14), we can sketch a set of curves showing the relationship between duty ratio D and voltage gain of V_o/V_i for different values of turns ratio n , as illustrated in Fig 6.

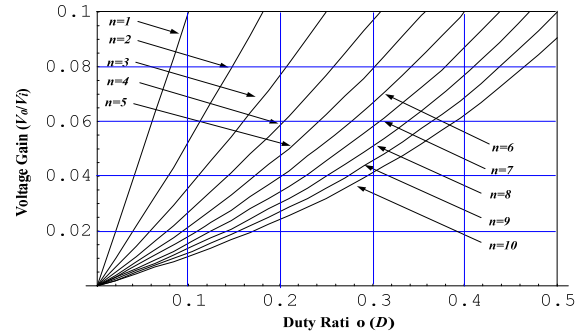


Fig. 6. Plots of V_o/V_i versus duty ratio D .

2.2.2 Voltage Stresses of Diode and Active Switch

At Mode 1 (as Fig. 5a), free-wheeling diode D_1 and active switch M_2 stay in the off state, while D_2 and M_1 are conducting. At Mode 5 (as Fig. 5b), the states of D_1 and D_2 as well as M_1 and M_2 are exchanged. Thus, their voltage stress can be represented as

$$V_D = \frac{(V_i - V_o)}{n} + V_o, \quad (15)$$

and

$$V_{DS} = V_i + (n - 1)V_o, \quad (16)$$

where V_D and V_{DS} stand for the voltage stresses of the diode and the active switch, in turn. From (15) and (16), we can sketch a set of curves showing the free-wheeling diode and active switch versus different values of turns ratio n , respectively, as shown in Fig. 7 and Fig. 8.

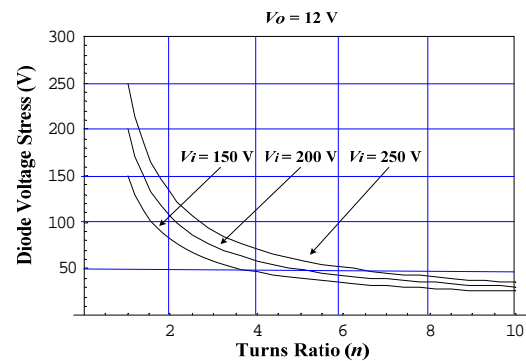


Fig. 7. Plots of diode voltage stress versus turns ratio n of the coupled inductor.

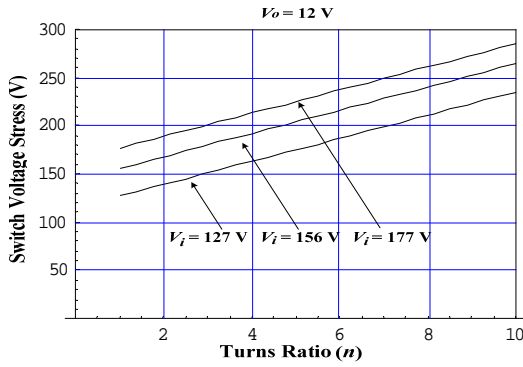


Fig. 8. Plots of switch voltage stress versus turns ratio n of the coupled inductor.

To objectively judge the merits of the proposed ICBC, performance comparison between the proposed ICBC and the IBC is summarized in Table 1. In addition, an ICBC with $n = 8$ is considered as an example for illustration, of which duty ratio, diode voltage stress, and switch voltage stress are compared with those of the IBC, shown in Fig. 9. From the plots in Fig. 9, it can be seen that the proposed ICBC yields higher duty ratio and lower diode voltage stress over the IBC.

Table 1. Comparison between the IBC and the proposed converter.

	IBC	the proposed converter
Voltage Gain	$\frac{V_o}{V_i} = D_m$	$\frac{V_o}{V_i} = \frac{D_n}{D_n + n(1 - D_n)}$
Duty Ratio	$D_m = \frac{V_o}{V_i}$	$D_n = \frac{nV_o}{V_i + nV_o - V_o}$
Diode Voltage Stress	$V_D = V_i$	$V_D = \frac{(V_i - V_o)}{n} + V_o$
Switch Voltage Stress	$V_{DS} = V_i$	$V_{DS} = V_i + (n - 1)V_o$

Note: D_m and D_n are the maximum duty ratio of the IBC and the proposed converter under identical input voltage, respectively.

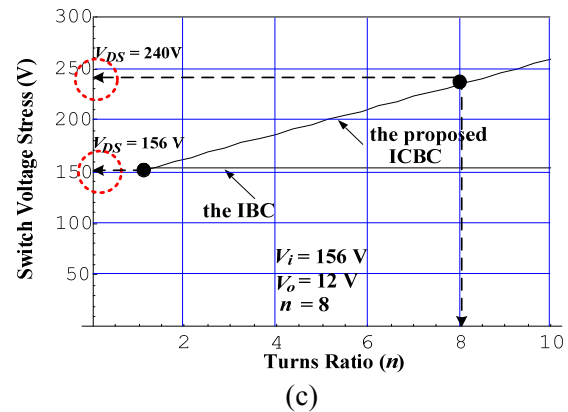
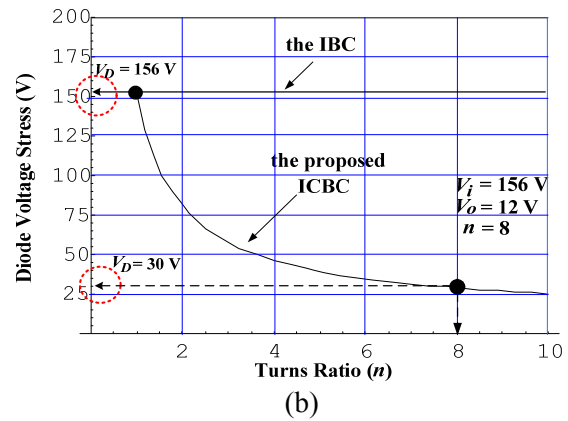
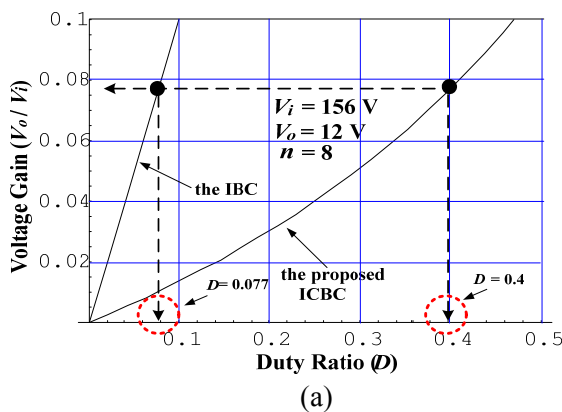


Fig. 9. Performance comparison between the proposed converter and the IBC: (a) duty ratio, (b) voltage stress of the diode and (c) voltage stress of the active switch.

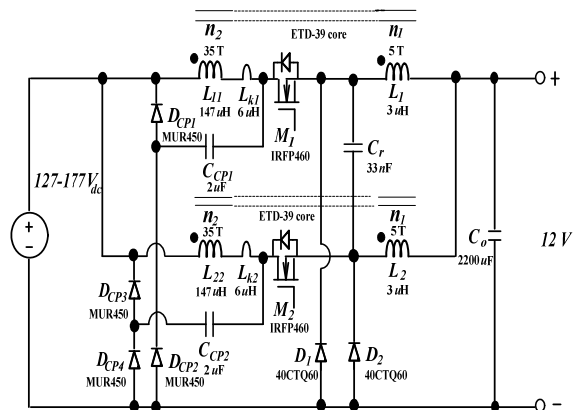


Fig. 10. Experimental circuit of the proposed ICBC

3 Design Considerations and Efficiency Estimation

To verify the feasibility, a 240 W prototype of the proposed soft-switching ICBC is designed and built, of which component values, part identification codes are shown in Fig. 10. In addition, its specifications are listed as follows:

- input voltage: 127-177 V_{dc}
- output voltage: 12 V_{dc}
- output current: 20 A
- switching frequency: 75kHz, and
- output power: 240 W

As followed are the design considerations for the proposed converter.

3.1 Design Considerations

A larger duty ratio D corresponds to a larger coupled-inductor turns ratio n , which results in a lower voltage stress on free-wheeling diodes D_1 and D_2 . In order to accommodate variations of loads, a proper turns ratio n of the coupled inductors is needed. From Fig. 6, we can obtain a proper coupled-inductor turns ratio $n = 8$. Its maximum duty ratio is $D_{max} \approx 0.46$ under input voltage $V_i = 127$ V_{dc} and minimum duty ratio is $D_{min} \approx 0.37$ under input voltage $V_i = 177$ V_{dc}.

3.1.1 Design of the Coupled Inductors

Once the coupled-inductor turns ratio $n = 8$ is selected, the minimum duty ratio can be determined as $D_{min} \approx 0.37$ under input voltage $V_i = 177$ V_{dc}. The maximum current ripple of the coupled inductors is designed with $i_{L(ripple)} = i_{L1(ripple)} = i_{L2(ripple)} = 6$ A. Thus, inductance $L = L_1 = L_2$ can be determined as

$$L = \frac{(V_{i(max)} - V_o)D_{min}}{n^2 i_{L(ripple)} f_s} \quad (17)$$

$$= \frac{(177-12)0.37}{64 \times 6 \times 75 \times 10^3} = 2.2 \mu\text{H},$$

where f_s is the switching frequency of the active switches. Suppose that inductance $L = 3 \mu\text{H}$ is selected in the design, if the turns ratio $n = (n_1+n_2)/n_1$ is equal to 8, the inductance $L_{11} = L_{22}$ can be found as

$$L_{11} = L_{22} = (n-1)^2 L \quad (18)$$

$$= 7^2 \times 3\mu = 147 \mu\text{H}.$$

Referring to TDK data book, we choose an optimum ferrite material PC40 with maximum flux density $B_{max} = 200$ mT. In addition, maximum winding factor $K_{w(max)}$ equals 0.4 and maximum current density J_{max} is 400 A/cm². Thus, the area product of the core can be obtained by the following equation:

$$A_p = W_a A_e > \frac{(P_o + \frac{P_o}{\eta}) \times 10^4}{B_{max} K_{w(max)} J_{max} f_s} = 2.1 \text{ cm}^4, \quad (19)$$

where W_a is the window area of the core, A_e expresses the effective cross-section area of the core, P_o stands for the output power of the converter and η denotes the efficiency. Based on the outcome of preceding calculations, we select core TDK ETD-39 ($A_e = 1.25$ cm², $W_a = 2.57$ cm², $V_e = 11.5$ cm³ and $A_L = 3150$ nH/N²), which can meet dimension requirement so as to reduce winding current density and to lower core temperature.

By applying the Faraday's law, turns (n_2) of the coupled inductor (L_{11} or L_{22}) is determined by

$$n_2 \geq \frac{V_{i(min)} D_{max}}{B_{max} A_e f_s} = 31.2. \quad (20)$$

In this design, n_2 is chosen as 35 turns. Then, with the relationship of $n = (n_1+n_2)/n_1$, the turns (n_1) of the coupled inductor (L_1 or L_2) can be correspondingly determined as

$$n_1 = \frac{n_2}{(n-1)} = 5. \quad (21)$$

3.1.2 Selection of Power Switches and Diodes

According to (15) and (16), the maximum voltage stress imposed on both free-wheeling diodes D_1 and D_2 is

$$V_{D(max)} = \frac{(V_{i(max)} - V_o)}{n} + V_o = 32.6 \text{ V}, \quad (22)$$

and on both active switches M_1 and M_2 is

$$V_{DS(max)} = V_{i(max)} + V_o (n-1) = 261 \text{ V}. \quad (23)$$

When active switch M_1 or M_2 is turned on, the peak switch current $i_{DS(peak)}$ can be given as

$$i_{DS(peak)} \approx \frac{I_o}{4} + \frac{1}{2} \frac{(V_{i(max)} - V_o) D_{min}}{n^2 L f_s} = 7.1 \text{ A}, \quad (24)$$

While free-wheeling diode D_1 or D_2 is conducting, the peak diode current $i_{D(peak)}$ can be approximated by the following equation:

$$i_{D(peak)} \approx \frac{I_o}{4} + \frac{1}{2} \frac{V_o (1 - D_{min})}{L f_s} = 21.8 \text{ A}. \quad (25)$$

Selection of switching devices M_1 and M_2 involves a trade-off between conduction loss and switching loss. The selection of MOSFETs with low $R_{ds(on)}$ will reduce conduction loss, but it will result in high parasitic capacitance. Switches with lower $R_{ds(on)}$ also imply larger die size and higher cost. For this application, we can select the proper MOSFETs as the IRFP460, which provide high enough safety margins with a drain-source breakdown voltage of 500 V. Several important parameters of the IRFP460 are listed as follows:

$V_{DSS} = 500$ V, $R_{ds(on)} = 0.27$ Ω , $C_{oss} = 870$ pF and $I_D = 20$ A. According to (22) and (25), in the selection of free-wheeling diodes D_1 and D_2 , a 40A/60V Schottky diode which has the lowest forward voltage drop can be employed. The Schottky diode 40CPQ60 manufactured by International Rectifier with a maximum dc reverse voltage $V_{RRM} = 60$ V and a forward voltage drop $V_{F(max)} = 0.49$ V is a good choice for D_1 and D_2 .

3.1.3 Selection of Clamp Capacitors

The voltage spike across the active switch (M_1 or M_2) is caused from the leakage inductance (L_{k1} or L_{k2}) and the output capacitance of the active switch. When the active switch is turned off and the free-wheeling diode is conducting, the leakage inductance and the output capacitor of the active switch form a resonant circuit. The energy trapped in leakage inductance is transferred to the output capacitance of the active switch, which causes a high voltage spike across the active switch. The maximum voltage stress of the active switch can be estimated as

$$V_{DS(max)} = V_i + (n-1)V_o + \frac{L_k i_{DS}^2}{2C_{CP} V_{CP}}. \quad (26)$$

When the clamp capacitor is large enough, the first two items in (26) dominate the turn-off voltage spike. In this study, clamp capacitors $C_{CP1} = C_{CP2} = 2\mu\text{F}/400\text{V}$ are selected.

3.2 Efficiency Estimation

Power loss of the proposed converter is also estimated to verify the measured efficiency. In Section 3.1, we have determined the key parameters of the ICBC. Their values are labeled in Fig. 10 and then, used for power loss evaluation and implementation.

3.2.1 Active Switches (M_1 and M_2)

The active switches of the proposed converter are designed to achieve ZVT at turn-off transition, so that their turn-off loss is negligible. Turn-on loss and conduction loss of the active switches can be determined from their switch voltage V_{DS} , switch current i_{DS} and channel resistance $R_{ds(on)}$. In the proposed converter, the MOSFETs used are IRFP460, and their channel resistance $R_{ds(on)}$ equals 0.27 Ω . Thus, turn-on loss and conduction loss of the active switches are approximated by

$$\begin{aligned} P_{loss(turn-on)}^{Switch} &\approx 2 \left[\frac{t_{on}}{2T_s} V_{DS(peak)} i_{DS(peak)} \right] \\ &= 2 \left(\frac{40n}{2} \times 75k \times 261 \times 7.1 \right) = 5.6 \text{ W}, \end{aligned} \quad (27)$$

and

$$\begin{aligned} P_{loss(Con)}^{Switch} &\approx 2 \left[\frac{1}{3} D_{\min} (i_{DS(peak)})^2 R_{ds(on)} \right] \\ &= \frac{2}{3} [0.37 \times (7.1)^2 \times 0.27] = 3.4 \text{ W}. \end{aligned} \quad (28)$$

Total power loss of the active switches is therefore

$$\begin{aligned} P_{Total}^{Switch} &= P_{loss(turn-on)}^{Switch} + P_{loss(Con)}^{Switch} \\ &= 5.6 + 3.4 = 9 \text{ W}. \end{aligned} \quad (29)$$

3.2.2 Free-wheeling Diodes (D_1 and D_2)

The free-wheeling diodes are selected as Schottky diodes of 40CPQ60, and their forward voltage drop $V_F = 0.49$ V. Thus, total conduction loss of the free-wheeling diodes can be determined as

$$\begin{aligned} P_{loss}^{Diode} &= 2 \left(\frac{I_o}{2} \right) V_F (1 - D_{\min}) \\ &= 2 \left(\frac{20}{2} \right) \times 0.49 (1 - 0.37) = 6.2 \text{ W} \end{aligned} \quad (30)$$

3.2.3 Coupled Inductors (L_1 and L_2)

According to the determination in Section 3.1.1, the cores of the coupled inductors are designed as TDK PC-40 ETD-39 ($A_e = 1.25\text{cm}^2$, $A_w = 2.57\text{cm}$, and $V_e = 11.5\text{cm}^3$) with maximum flux density $B_{max} = 200$ mT. Additionally, winding turns in the primary are $n_p = (n_1 + n_2) = 40$, in the secondary are $n_s = n_1 = 5$, and the turns ratio is $n = n_p/n_s = 8$. Thus, from Fig. 11, we can find the inductor core loss per cubic

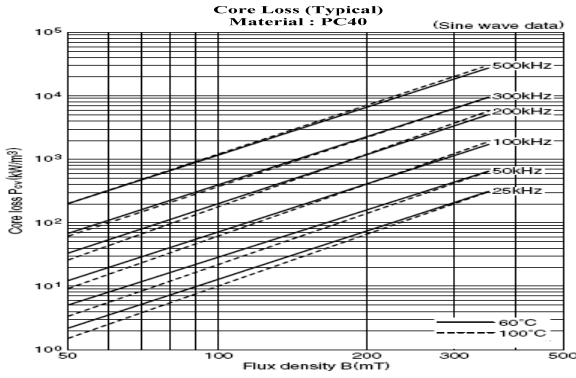


Fig. 11. Typical core loss data of the coupled inductors.

centimeter, that is, $P_{Coup(cv)} = 0.2 \text{ W/cm}^3$ at $60 \text{ }^\circ\text{C}$. The total core loss of each coupled inductor will be

$$P_{core}^{Coup} = P_{Coup(cv)} \times V_e = 0.2 \times 11.5 = 2.3 \text{ W.} \quad (31)$$

The measured winding resistance of the coupled inductors is $R_{Coup} = 76 \text{ m}\Omega$, which is adopted to estimate copper loss as follows:

$$P_{copper}^{Coup} = \left(\frac{I_o}{2}\right)^2 R_{Coup} \quad (32)$$

$$= \left(\frac{20}{2}\right)^2 \times 76 \times 10^{-3} = 7.6 \text{ W.}$$

Total power loss of the coupled inductors is therefore

$$P_{Total}^{Coup} = 2(P_{core}^{Coup} + P_{copper}^{Coup}) \quad (33)$$

$$= 2(2.3 + 7.6) = 19.8 \text{ W.}$$

Finally, the estimated total power loss and efficiency of the proposed converter at input voltage $V_i = 177 \text{ V}_{dc}$ are determined as

$$P_{loss}^{Total} = P_{Total}^{Switch} + P_{Total}^{Diode} + P_{Total}^{Coup} = 35 \text{ W,} \quad (34)$$

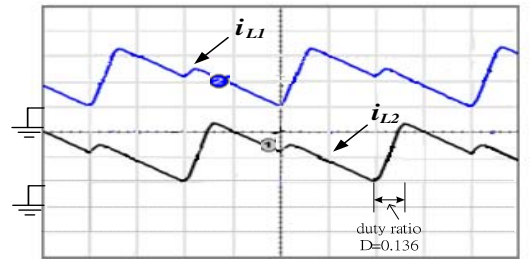
and

$$\eta_{\%}^{\max} = \frac{P_{out}}{P_{out} + P_{loss}^{Total}} \quad (35)$$

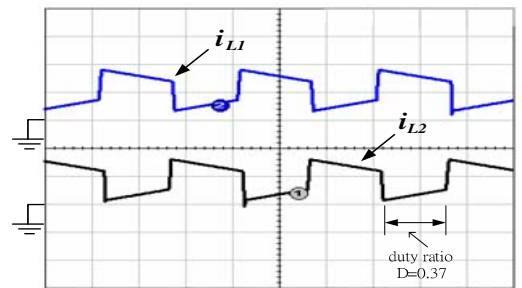
$$= \frac{240}{240 + 35} = 87.3 \text{ \%}.$$

4 Simulated and Experimental Results

The proposed ICBC is simulated and measured for verification. Fig. 12 shows simulated inductor current waveforms of the conventional IBC and the proposed ICBC, it can be seen that the proposed ICBC can extend duty ratio effectively. Fig. 13 shows measured inductor current waveforms of the proposed ICBC. Fig. 14 shows simulated and experimental waveforms of the active switches in the ICBC. It can be seen that there is no any spike voltage across the active switches. That is, the energy trapped in the leakage is recycled. Fig. 15(a) and (b) show expanded waveforms of the active switch voltage and current with respect to turn-on and turn-off transitions, from which it can be seen that the switching loss is reduced, particularly in turn-off transition. Fig. 16 shows measured waveforms of the voltage and current of the free-wheeling diode. It can be found that the free-wheeling diode has featured low voltage stress and low reverse-recovery loss. Fig. 17 shows the efficiency measurements of the proposed soft-switching ICBC. It is apparent that the proposed converter can achieve a high efficiency up to 85% under full load condition.

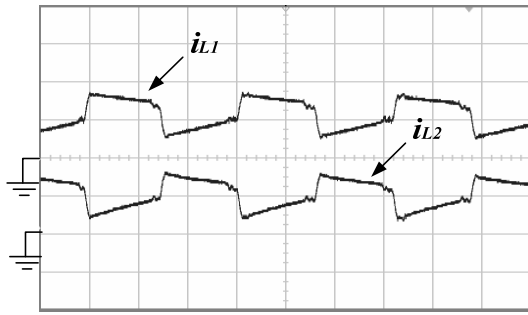


(i_{L1} : 10A/div, i_{L2} : 10A/div, Time: $5\mu\text{s/div}$)
(a)



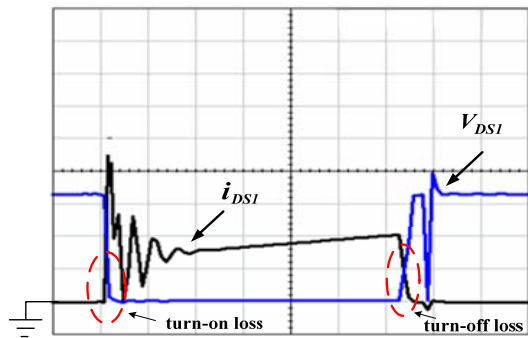
(i_{L1} : 10A/div, i_{L2} : 10A/div, Time: $5\mu\text{s/div}$)
(b)

Fig. 12. Simulated waveforms of inductor currents i_{L1} and i_{L2} : (a) the conventional IBC, (b) the proposed ICBC.

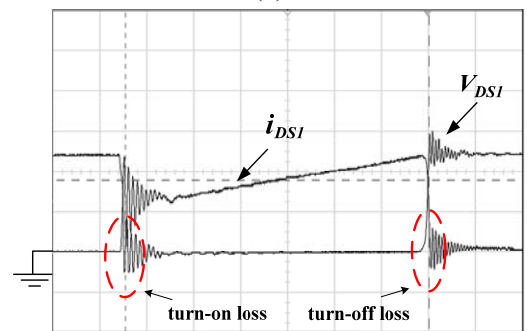


(i_{L1} : 10A/div, i_{L2} : 10A/div, Time: 5 μ s/div)
(b)

Fig. 13. Measured waveforms of inductor currents i_{L1} and i_{L2} of the proposed ICBC.

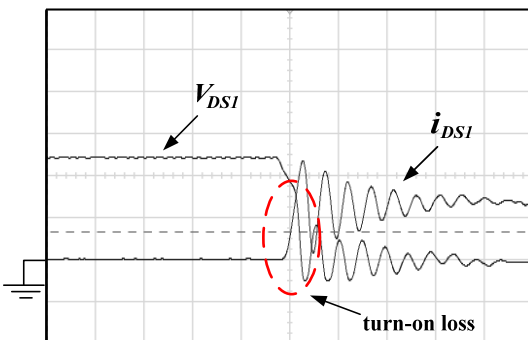


(V_{DS1} : 100V/div, i_{DS1} : 5A/div, Time: 1 μ s/div)
(a)

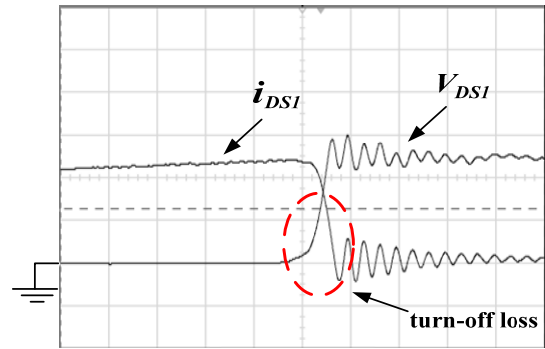


(V_{DS1} : 100V/div, i_{DS1} : 5A/div, Time: 1 μ s/div)
(b)

Fig. 14. Voltage and current waveforms of active switches: (a) simulated results, (b) experimental results.

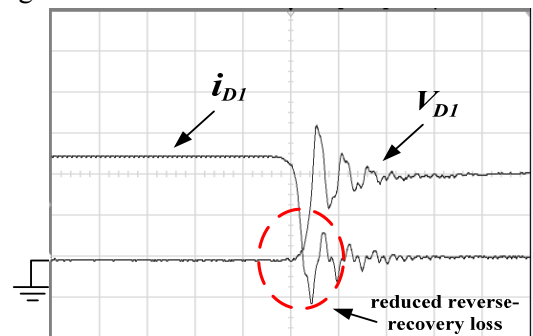


(V_{DS1} : 100 V/div, i_{DS1} : 5 A/div, Time: 200 ns/div)
(a)



(V_{DS1} : 100 V/div, i_{DS1} : 5 A/div, Time: 200 ns/div)
(b)

Fig 15. Expanded voltage and current waveforms of active switches: (a) during turn-on transition, (b) during turn-off transition.



(V_{DI} : 20 V/div, i_{DI} : 10 A/div, Time: 200 ns/div)

Fig 16. Measured voltage and current waveforms of the free-wheeling diodes.

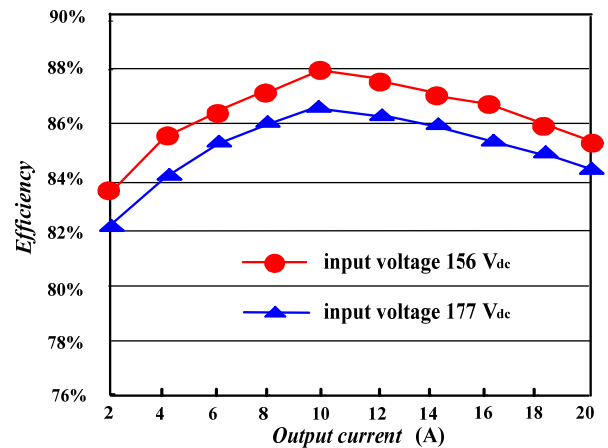


Fig 17. Plots of efficiency versus output current for the proposed soft-switching converter with different input voltages.

5 Conclusions

In this paper, the proposed soft-switching ICBC has been analyzed and implemented. The proposed converter with coupled inductors can extend duty ratio of the active switch and reduce component

stress. To handle the energy trapped in the leakage inductance of the coupled inductors, a simple passive-clamp circuit is added to the proposed converter, which can effectively recycle the energy and suppress voltage spike. With the proposed converter, conversion efficiency therefore can be improved significantly.

In this paper, analysis of the proposed converter has been presented in detail, including operational principle and characteristics. To verify the feasibility of the proposed converter, design consideration and power loss estimation are also discussed. An experimental prototype for the proposed converter is built and evaluated. Experimental results have demonstrated that the proposed ICBC can achieve high efficiency over a wide load range. Compared with the conventional IBC, it improves efficiency by 1.5%. The proposed ICBC is relatively suitable for non-isolation, high step-down voltage and low output current ripple applications.

References:

- [1] Hong Mao, *et al.*, "Analysis of Inductor Current Sharing in Non-isolated and Isolated Multiphase dc-dc Converters," *IEEE Transactions on Industrial Electronics*, Vol. 54, No. 6, Dec. 2007, pp. 3379-3388.
- [2] M. López, *et al.*, "Current Distribution Control Design for Paralleled DC/DC Converters Using Sliding Mode Control," *IEEE Transactions on Industrial Electronics*, Vol. 51, No. 2, Apr. 2004, pp. 419-428.
- [3] Xiong Du, Luwei Zhou, and Heng-Ming Tai, "Double-Frequency Buck Converter," *IEEE Transactions on industrial Electronics*, Vol. 56, No. 5, May 2009, pp. 1690-1698.
- [4] Shen-Yaur Chen and Jin-Jia Chen, "Study of the Effect and Design Criteria of the Input Filter for Buck Converters with Peak Current-Mode Control Using a Novel System Block Diagram," *IEEE Transactions on Industrial Electronics*, Vol. 55, No. 8, Aug. 2008, pp. 3159-3166.
- [5] J. J. Lee and B. H. Kwon, "DC-DC Converter Using a Multiple-Coupled Inductor for Low Output Voltages," *IEEE Transactions on Industrial Electronics*, Vol. 54, No. 1, Feb. 2007, pp. 467-478.
- [6] P. L. Wong, P. Xu, B. Yang, and F. C. Lee, "Performance Improvements of Interleaving VRMs with Coupling Inductors," *IEEE Transactions on Power Electronics*, Vol. 16, No. 4, Jul. 2001, pp. 499-507.
- [7] Peng Xu, Jia Wei, and Fred C. Lee, "Multiphase Coupled-Buck Converter—A Novel High Efficient 12 V Voltage Regulator Module," *IEEE Transactions on Power Electronics*, Vol. 18, No. 1, Jan. 2003, pp. 74-82.
- [8] Milan Ilic and Dragan Maksimovic, "Interleaved Zero-Current-Transition Buck Converter," *IEEE Transactions on Industry Applications*, Vol. 43, No. 6, Nov. 2007, pp. 1619-1627.
- [9] Chu-Yi Chiang and Chern-Lin Chen, "Zero-Voltage-Switching Control for a PWM Buck Converter under DCM/CCM Boundary," *IEEE Transactions on Power Electronics*, Vol. 24, No. 9, Sep. 2009, pp. 2120-2126.
- [10] Yaow-Ming Chen, *et al.*, "Interleaved Buck Converters with a Single-Capacitor Turn-Off Snubber," *IEEE Transactions on Aerospace and Electronic System*, Vol. 40, No. 3, July 2004, pp. 954-967.
- [11] K. Yao, *et al.*, "Tapped-Inductor Buck Converter for High-Step-Down DC-DC Conversion," *IEEE Transactions on Power Electronics*, Vol. 20, No. 4, 2005, pp. 775-780.
- [12] K. Yao, *et al.*, "Tapped Inductor Buck Converters with a Lossless Clamp Circuit," *Proceedings of the Applied Power Electronics Conference*, Vol. 2, 2002, pp. 693-698.
- [13] P. Xu, J. Wei and F. C. Lee, "The Active-Clamp Couple-Buck Converter-A Novel High Efficiency Voltage Regulator Module," *Proceedings of the Applied Power Electronics Conference*, Vol. 1, 2001, pp. 252-257.
- [14] E.-S. Kim, *et al.*, "An Improved Soft-Switching PWM FB DC/DC Converter for Reducing Conduction Losses," *IEEE Transactions on Power Electronics*, Vol. 14, No. 2, Mar. 1999, pp. 258-263.
- [15] Y. Jang, M. M. Jovanović, and Y. M. Chang, "A New ZVS-PWM Full-Bridge Converter," *IEEE Transactions on Power Electronics*, Vol. 18, No. 5, Sep. 2003, pp. 1122-1129.
- [16] R. Martinelli and C. Ashley, "Coupled Inductor Boost Converter with Input and Output Ripple Cancellation," *Proceeding of the Applied Power Electronics Conference*, 1991, pp. 567-572.